1

Definition, Function, and Design of Interface in Ceramic-Matrix Composites

1.1 Introduction

To realize the advantages of operating systems under high-temperature conditions, it is necessary to master the properties of a large number of high-temperature materials and components. For example, a significant increase in the gas temperature will significantly increase the gas turbine efficiency. The introduction of new materials and new technology has gradually improved the high-temperature performance of gas turbine engine for more than 70 years, but the development of cooling methods and solutions has contributed more than 75% to the performance improvement (Li 2018).

Although component cooling methods and engine material properties have improved significantly, most high-temperature alloys currently operate at temperatures above 90% of their original melting point. Higher operating temperatures are required for more efficient engines, which will require higher component temperatures. As the operating temperature continues to increase, new materials with higher thermo-mechanical and thermo-chemical properties are required to meet high-temperature structural applications. Ceramic-matrix composites (CMCs) are considered to have the potential to provide high strength, high toughness, creep resistance, low notch sensitivity, and environmental stability to meet the needs of future high-performance turbine engines (Li 2019).

Figure 1.1 shows the tensile stress–strain curve of monolithic ceramic and fiber-reinforced CMCs. For a monolithic ceramic material, when it is subjected to tensile stress, it appears as elastic deformation at low stress level; as the stress increases, cracks occur in the defect region of the material, and the cracks rapidly expand, causing the material to undergo brittle fracture. When the CMC material is subjected to tensile stress, it is elastically deformed before matrix cracks; as the tensile stress increases, the matrix begins to crack, and the fibers begin to debond and play a role of crack bridging; as the tensile stress increases further, the cracks become saturated, and the bridging fibers begin to pull out; as the tensile stress continues to increase, the fibers begin to break until the material reaches the highest strength. The fracture modes of monolithic ceramics and CMCs are different, mainly because the interface plays a role in the fracture process of CMCs. The interface is a special domain between the matrix

Interfaces of Ceramic-Matrix Composites: Design, Characterization and Damage Effects,
First Edition. Longbiao Li. © 2020 WILEY-VCH GmbH.

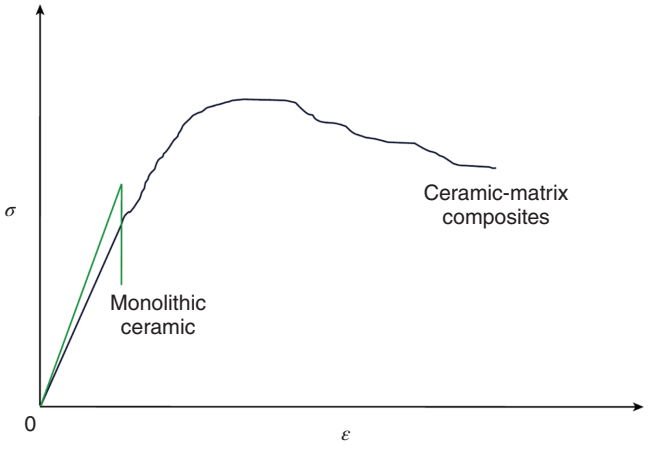

Figure 1.1 The tensile stress–strain curves of monolithic ceramics and fiber-reinforced CMCs.

and the reinforcement. It is the link between the fiber and the matrix, and also a bridge for load transfer. The structure and properties of interphase directly affect the strength and toughness of CMCs.

1.2 The Definition of Interface in Ceramic-Matrix Composites

CMCs possess good damage tolerance, mainly due to frictional sliding at the fiber–matrix interface, and the interphase enables frictional sliding to occur between the fiber and the matrix. The damage tolerance is manifested in CMC with 1% ductility, and the sensitivity to notches is comparable with that of aluminum alloys. CMCs also exhibit good room-temperature fatigue resistance. The fatigue strength (i.e. fatigue failure does not occur when the stress is less than the fatigue strength) is about 90% of the ultimate tensile strength, but the fatigue damage increases with temperature. The tensile strength of CMCs is usually volume-stable as the damage tolerance ability of CMCs decreases the scaling effect that often occurs in the monolithic ceramic materials due to the weakest link. Due to crack deflection and crack tip resistance, CMCs can have cracks that can cause catastrophic failure of monolithic ceramics without fracture. This thermomechanical performance is particularly suitable for producing large, static load, and high-temperature structural components.

CMCs can be divided into two types, i.e. oxide materials and non-oxide materials. Oxide composites include oxide fibers (e.g. Al_2O_3), interphase, and matrix. If any of the aforementioned three components contains non-oxide material (for example, SiC), the composite is classified as non-oxide CMC.

A lot of research and development work is conducted on non-oxide CMCs, especially SiC fiber-reinforced SiC matrix composite (SiC/SiC CMC) using pyrolytic carbon (PyC) or boron nitride (BN) as the fiber interface layer.

Non-oxide CMCs have good high-temperature properties, such as creep resistance and microstructure stability. They also have high thermal conductivity and low thermal expansion, which show a good resistance to thermal stress. SiC/SiC composites are very suitable as thermal load components, such as chamber throat, flap, blade, and heat exchanger. Oxide CMCs (for example, oxide fiber-reinforced porous oxide-matrix composite without interphase) have excellent oxidation resistance, resistance to alkaline corrosion, low dielectric constant, and low price.

Both oxide and non-oxide CMCs exhibit some disadvantages. Non-oxide CMCs (for example, SiC/SiC) exhibit brittleness at intermediate temperatures (about 700 °C). Brittleness is more severe under cyclic loading conditions as oxygen enters from the cracks in the matrix and reacts with the interphase and fibers forming oxidation products, leading to the propagation of the matrix cracks. These oxidation reaction products limit the friction sliding mechanism between the fiber and the matrix inside the material, which can improve the toughness of CMCs. Although this oxidation effect does not occur when the stress is below the proportional limit stress, design and operation experience has shown that it is necessary to consider in advance that the overload stress exceeds the proportional limit stress. Therefore, the local brittleness has become the main limitation of non-oxide CMCs.

Compared with SiC/SiC, oxide CMCs do not undergo oxidation embrittlement, but have a temperature limit (about 1000 °C), which is related to creep and sintering. Moreover, the interface technology of oxide CMCs is less mature than that of non-oxide CMCs. The performance data of most oxide CMCs are obtained in systems without interphase, and the damage tolerance is based on a porous matrix.

1.2.1 Non-oxide CMCs

SiC/SiC CMCs maintain the advantages of SiC matrix such as high-temperature resistance, high strength, low density, and oxidation resistance, realize the strengthening and toughening effect of SiC fiber, and effectively overcome the fatal disadvantages of monolithic ceramics that are brittle, crack sensitivity, and low reliability. Compared with superalloys, SiC/SiC CMCs have lower density (usually 2.0–3.0 g/cm^3, only 1/3–1/4 of superalloys) and higher temperature resistance (>1200 °C under non-cooling conditions) (Liu et al. 2018).

After decades of research, a variety of CMC preparation processes have been developed. Representative processes include chemical vapor infiltration (CVI), polymer infiltration and pyrolysis (PIP) process, and melt infiltration (MI). The main difference between the three processes is the densification of the SiC matrix.

(1) CVI process uses a gaseous precursor (for example, trichloromethylsilane) to pyrolysis and deposit on the surface of the SiC fiber to obtain an SiC matrix.
(2) PIP process usually infiltrates the fiber preform in liquid precursors (such as polycarbosilane), the precursors are ceramicized by high-temperature pyrolysis, and the infiltration and pyrolysis process is repeated to obtain a dense SiC matrix.

(3) Reactive melt infiltration (RMI) is the infiltration of molten silicon into a porous carbon preform, and the reaction of carbon and silicon generates an SiC matrix.
(4) Non-reactive melt infiltration infiltrated the molten silicon into the pores of the matrix, which mainly plays a filling role, and no reaction between silicon and carbon occurs.

The fundamental physical and mechanical properties of SiC/SiC composites prepared by different processes are shown in Table 1.1.

In-plane tensile performance is one of the most important mechanical properties and reflects the strength of the composite material to resist the damage of external tensile load.

Figure 1.2 shows the tensile stress–strain curve of Prepreg-MI SiC/SiC composites (Corman et al. 2016). The curve can be divided into four stages:

- Stage I is the elastic region, and the strain increases proportionally with the stress.
- Stage II is the damage region with a large number of microcracks generated in the matrix of the composite material, and the fibers are debonded. The behavior of matrix cracking and fiber debonding attributes "pseudoplastic" and high toughness of CMCs.
- Stage III is the damage region with saturation of matrix cracking, and the fiber is completely debonded from the matrix.
- Stage IV is where the fiber breaks under higher stress.

The stress–strain curve can be used to obtain Young's modulus, proportional limit stress, ultimate strength, fracture strain, and other related data of the composite material. The proportional limit stress is particularly important, which reflects the maximum stress experienced by the matrix before the generation of matrix microcracks, and is usually defined as the maximum design stress of the component.

There are many factors affected the in-plane tensile performance of SiC/SiC composite, i.e. the type of SiC fiber and fiber volume fraction, as shown in Table 1.2. For the Hi-Nicalon™ S and Tyranno™ SA3 reinforced SiC matrix composites, at the same fiber volume fraction of $V_f = 34.8\%$, the ultimate tensile strength and fracture strain are much higher, and the initial modulus and proportional limit stress are much lower for Hi-Nicalon S SiC/SiC composite than those of Tyranno SA3 SiC/SiC composite. For the SiC/SiC composite with the same fiber and preparation process, i.e. Hi-Nicalon S SiC-SiC MI-CMC or Sylramic™-iBN SiC/SiC PIP-CMC, the ultimate tensile strength increases with fiber volume fraction. The in-plane mechanical properties of SiC/SiC composite are also affected by the temperature. For the Prepreg-MI Hi-Nicalon SiC/SiC composite, when the testing temperature increases from 25 to 1200 °C, the composite initial modulus (E_c) decreases, i.e. from 285 to 243 GPa; the proportional limit stress (σ_{pls}) remains stable, i.e. between 165 and 167 MPa; and the ultimate tensile strength (σ_{UTS}) decreases with increasing temperature, i.e. from 321 to 224 MPa; and the fracture strain (ε_f) is very sensitive to the temperature, and decreases from 0.89% to 0.31%.

Table 1.1 Fundamental physical and mechanical properties of SiC/SiC composites prepared by different processes.

Parameter	CVI		MI						CVI + PIP
	SNECMA		NASA		GE				NASA
	—		N22	N24-A	HiPerComp/Prepreg		HiPerComp/Slurry cast		N26-A
Fiber type	Nicalon		Sylramic	Sylramic-iBN	Hi-Nicalon		Hi-Nicalon		Sylramic-iBN
Fiber volume fraction (%)	40		36	36	22–40		35–38		36
Testing temperature (°C)	23	1000	20	20	25	1200	25	1200	20
Density (g/cm^3)	2.5	2.5	2.85	2.85	2.80	2.76	2.70	2.66	2.52
Porosity (%)	10	10	2	2	<2	—	6	—	14
Thermal conductivity (‖) (W/(m K))	19	15.2	—	—	33.8	14.7	30.8	14.8	—
Thermal conductivity (⊥) (W/(m K))	9.5	5.7	24 (204 °C)	30 (204 °C)	24.7	11.7	22.5	11.8	26 (204 °C)
			15 (1204 °C)	14 (1204 °C)					10 (1204 °C)
Coefficient of thermal expansion (‖) (10^{-6}/K)	3	3	—	—	3.73 (25–1200 °C)		4.34 (25–1200 °C)		—
Coefficient of thermal expansion (⊥) (10^{-6}/K)	1.7	3.4	—	—	4.15 (25–1200 °C)		3.12 (25–1200 °C)		—
Initial modulus (GPa)	230	200	250	250	285	243	196	144	200
Proportional limit stress (MPa)	—	—	180	180	167	165	120	130	130
Ultimate strength (MPa)	200	200	400	450	321	224	358	271	330
Strain to failure (%)	0.3	0.4	0.35	0.5	0.89	0.31	0.74	0.52	0.40
Interlaminar tensile strength (MPa)	—	—	—	—	39.5	—	—	—	—
Interlaminar shear strength (MPa)	40	35	—	—	135	124	—	—	—
Flexural strength (MPa)	300	400	—	—	—	—	—	—	—
In-plane compressive strength (MPa)	580	480	—	—	1190	>700	—	—	—

NASA, National Aeronautics and Space Administration; GE, General Electric Company.

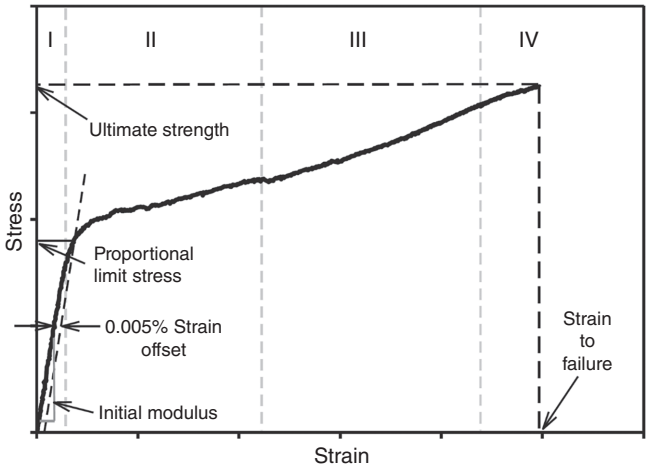

Figure 1.2 Typical tensile stress–strain behavior of Prepreg-MI SiC/SiC composite.

Table 1.2 In-plane tensile properties of SiC/SiC composite with BN interphase at room temperature.

Process	Fiber type	Volume fraction (%)	Elastic modulus (GPa)	Proportional limit stress (MPa)	Ultimate strength (MPa)	Strain to failure (%)
CVI	Hi-Nicalon S	27.7	273	108	273	0.39
	Sylramic-iBN	36.4	242 ± 18	150 ± 5	430 ± 6	0.52 ± 0.017
MI	Hi-Nicalon S	30.2	262	154	341	0.63
	Hi-Nicalon S	34.8	232	147	412	0.60
	Sylramic-iBN	38.9	260 ± 15	184 ± 19	468 ± 30	0.48 ± 0.03
	Tyranno SA3	34.8	254	152	358	0.33
PIP	Sylramic-iBN	52.6	161	133	431	0.35
	Sylramic-iBN	50.0	164	148	317	0.274

The fiber preform also affects the in-plane tensile performance, as shown in Table 1.3. For the 3D orthogonal unbalanced SiC/SiC composite, the fiber volume fraction is the highest along the loading direction (i.e. $V_{fl} = 28\%$), and the ultimate tensile strength is also the highest (i.e. $\sigma_{UTS} > 575$ MPa). For the 3D layer-to-layer angle interlock SiC/SiC composite, the fiber volume fraction is the lowest along the loading direction (i.e. $V_{fl} = 10\%$), and the ultimate tensile strength is also the lowest (i.e. $\sigma_{UTS} = 204$ MPa). When the fiber volume fraction along the loading direction increases, the SiC fiber with high modulus can carry more applied stress, which decreases the stress carried by the matrix and increases the matrix cracking stress. For the 2D triaxial braid composite, the fiber volume fraction along the loading direction is $V_{fl} = 26\%$, which is only slightly lower than that of

Table 1.3 In-plane tensile properties of SiC/SiC composites with different fiber preforms.

Architecture type	Architecture description	Volume fraction in load direction (%)	Elastic modulus (GPa)	Proportional limit stress (MPa)	Ultimate strength (MPa)	Average stress on fibers at failure (MPa)
AI UNI	1D angle interlock through the thickness, Y aligned, unbalanced	23	305 ± 4	322 ± 7	>472	>2052
BRAID	2D triaxial braid (double tow)	26	250 ± 10	245 ± 14	352 ± 18	1352
2D5HS	2D five-harness stain, balanced 0/90 lay-up	19	250	175	463	2362
2D 5HS DT	2D five-harness satin (double tow), balanced 0/90 lay-up	19	197	142	480	2526
LTLAI	3D layer-to-layer angle interlock	10	125	89	204	2040
3DO-Un-R	3D orthogonal, unbalanced	28	275 ± 9	261 ± 16	>575	>2053

3D orthogonal unbalanced composite (i.e. $V_{fl} = 28\%$). However, the tensile ultimate strength is much lower than expected due to the characteristics of shear failure. For the 2D five-harness stain composite, the average stress on fibers at failure is the highest (i.e. 2526 MPa), which indicates that this fiber preform can better realize the loading carry capacity of the fiber.

At high temperature ($T > 900\,^{\circ}C$), SiC may undergo either active or passive oxidation (Roy et al. 2014; Nasiri et al. 2016). At low oxygen pressure (<1 atm), active oxidation occurs due to the formation of volatile products, as follows:

$$SiC(s) + 2SiO_2(s) \rightarrow 3SiO(g) + CO(g) \tag{1.1}$$

$$SiC(s) + O_2(g) \rightarrow SiO(g) + CO(g) \tag{1.2}$$

At high oxygen pressure, passive oxidation occurs, and a protective film of SiO_2 is formed on the surface according to:

$$SiC(s) + \frac{3}{2}O_2(g) \rightarrow SiO_2(g) + CO(g) \tag{1.3}$$

$$SiC(s) + 2O_2(g) \rightarrow SiO_2(s) + CO_2(g) \tag{1.4}$$

Oxidation can lead to the degradation of CMC performance, and the degradation behavior is much different for different SiC/SiC composites. For the Prepreg-MI Hi-Nicalon SiC/SiC composite, after exposure at 1200 °C in air atmosphere for 4000 hours, the ultimate tensile strength degrades about 10%. However, after exposure 1000 hours at 1315 °C in air atmosphere, the ultimate tensile strength degrades about 30%. For the Prepreg-MI Hi-Nicalon S SiC/SiC

composite, after exposure 4000 hours at 1315 °C in air atmosphere, the ultimate tensile strength degrades less than 10% (Corman et al. 2016).

Ünal et al. (1995) performed oxidation heat-treatment of the composite bars in flowing dried oxygen at 1400 °C for 50 hours. The cut edges of the bars were not sealed after machining, and they were directly exposed to the oxidizing environment, which represents an application case where the matrix is significantly cracked or machined surfaces are exposed. Mechanical testing was conducted at room temperature using a four-point bend fixture with 10 and 20 mm top and bottom span distances, respectively. Oxidation heat treatment of SiC/SiC composites at 1400 °C for 50 hours leads to the formation of the passive oxidation product of cristobalite (SiO_2). However, cristobalite does not seal surface completely, including pores, and there, it is not protective. Mechanical test results clearly demonstrate that oxidation reduces both the fracture stress and the cyclic life, at a given stress level, by about 50%. The degradation of the mechanical properties appears to be related to the preferential oxidation of PyC present at the fiber/matrix interface.

Morscher et al. (2000) investigated the tensile stress-rupture behavior of Hi-Nicalon reinforced MI SiC matrix composites with BN interphase in air at intermediate temperatures. The rupture properties of Hi-Nicalon, BN-interphase, and SiC-matrix composites showed significant loss in load-carrying ability compared with the expected load-carrying ability of the reinforcing fibers for the same temperatures and rupture times. Oxidation of the BN interphase and the formation of borosilicate oxidation products cause strength bonding between individual fibers at locations of near fiber-to-fiber contact. BN interphase oxidation appeared to be enhanced by the carbon layer formed at the Hi-Nicalon fiber surface during matrix processing. At higher stresses, a faster rate for rupture was observed. For this case, through-thickness cracks existed in the matrix due to the initial loading condition. Oxidation ingress occurred from around all sides and edges of matrix cracks into the interior of the composite. Embrittled fibers would fail and shed load onto the remaining fibers. When the load applied to the remaining, unoxidized fibers reached a failure criterion load, based on the reduced load-bearing area, the composite failed. At lower stresses, a slower rupture rate was observed. For this case, microcracks existed in the matrix due to the lower stress loading condition. These cracks would be oxidized and the fibers embrittled. As the embrittled fibers failed due to degradation and strong bonding, the microcracks would grow, shedding the loads of the embrittled fibers onto pristine regions of composite.

Rouby and Reynaud (1993) investigated the tension–tension cyclic fatigue behavior of 2D CVI-SiC/SiC composite at room temperature. The loading frequency is $f = 1$ Hz, and the stress ratio is $R = 0$. The fatigue peak stress is $\sigma_{max} = 50$–175 MPa, and the maximum cycle number is defined as $N = 1\,000\,000$. At room temperature, the fatigue limit stress is $\sigma_{lim} = 135$ MPa, which is 75% of the ultimate tensile strength. According to the different fatigue peak stresses at room temperature, the fatigue damage can be divided into three cases:

- Case I, when the fatigue peak stress is higher than the ultimate tensile strength, the composite is fractured upon first loading to the peak stress.

- Case II, when the fatigue peak stress is between the fatigue limit stress (75% of the ultimate tensile strength) and ultimate tensile strength, fatigue failure occurs within a certain number of applied cycles.
- Case III, when the fatigue peak stress is below the fatigue limit stress, the composite cannot fail within 1 000 000 applied cycles. However, when the fatigue peak stress is higher than the first matrix cracking stress, the shape of the stress–strain hysteresis loops changes with applied cycles.

Chawla et al. (1996) investigated the effect of interphase thickness on tension–tension cyclic fatigue behavior of 2D CVI Nicalon™ SiC/C/SiC composite at room temperature for different loading frequencies. The fibers were woven into a plain-weave fabric and coated with chemical vapor deposited (CVD), PyC. The thickness of the PyC interphase is 0.33 and 1.1 μm. The composites were tested at loading frequencies of $f = 100$ and 350 Hz, and the fatigue peak stress is $\sigma_{max} = 120$ and 150 MPa. Under the same fatigue peak stress, the fatigue life with thickness interphase is longer than that with thin interphase, and the temperature rising of thin interphase is much higher than that of thickness interphase. The composite with thickness interphase protects the fiber from interface wear under high loading frequency, leading to the decrease of surface temperature of composite and increase of fatigue lifetime.

Reynaud et al. (1994) and Reynaud (1996) investigated the cyclic tension–tension fatigue behavior of 2D woven SiC/SiC and cross-ply SiC/MAS-L (silicon carbide/magnesium aluminosilicate-L) composites at elevated temperature in inert atmosphere. For the SiC/SiC composite, the radial stress at the fiber/matrix interface is compressive stress; when the temperature increases, the radial compressive stress decreases, leading to the decrease of the interface shear stress, and the increase of hysteresis dissipated energy. For the cross-ply SiC/MAS-L composite, the radial stress at the fiber/matrix interface is tensile stress, and when the temperature increases, the radial tensile stress decreases, leading to the increase of the interface shear stress and the increase of hysteresis dissipated energy. At elevated temperature between 800 and 1000 °C in inert atmosphere, the chemical reaction occurs at the fiber/matrix interface, leading to the decrease of the interface shear stress. After heat treatment at elevated temperature in inert atmosphere for 50 hours, the interface shear stress decreases through the hysteresis analysis at room temperature.

Elahi et al. (1996) investigated the tension–tension fatigue behavior of 2D CVI Nicalon SiC/SiC composite at room temperature and 1000 °C in air environment. The fatigue life at elevated temperature is much less than that at room temperature. At room temperature, when the fatigue peak stress is 75% of tensile strength, the modulus decreases 50% at initial stage of cyclic loading, then remains stable, and the composite experienced 1 540 000 cycles without fatigue fracture, and the tensile strength remained unchanged, however, the modulus decreased 42%. At elevated temperature, the fatigue peak stress is 77.4% of tensile strength, and the modulus decreased 40% during initial cyclic loading, and then degraded slowly with applied cycles, and when the modulus degradation approached 50%, the composite fatigue fractured.

Ünal (1996a,1996b,1996c) investigated the tensile and fatigue behavior of 2D CVI Nicalon SiC/SiC composite at room temperature and 1300 °C in N_2 atmosphere. The loading frequency is $f = 0.5$ Hz and the stress ratio is $R = 0.1$. The maximum cycle number is defined as 10 000 cycles at room temperature, and 72 000 cycles at 1300 °C. At room temperature, the proportional limit stress is $\sigma_{pls} = 70$ MPa, and the tensile strength is $\sigma_{UTS} = 185$ MPa; however, at 1300 °C, the proportional limit stress is $\sigma_{pls} = 60$ MPa, and the tensile strength is $\sigma_{UTS} = 225$ MPa, and the fracture strain at 1300 °C is twice of that at room temperature, due to the creep damage of fiber. At room temperature, when the fatigue peak stress is $\sigma_{max} = 105$ and 150 MPa, the composite cycled 10 000 without fatigue failure; and when the fatigue peak stress is $\sigma_{max} = 190$ MPa, the composite cycled 422 and fatigue fractured, and the composite modulus degraded rapidly during initial 100 cycles. At elevated temperature of 1300 °C, when the fatigue peak stress is $\sigma_{max} = 72$ and 108 MPa, the composite cycled to the number of $N = 72\,000$ without failure; and when the fatigue peak stress is $\sigma_{max} = 145$ and 188 MPa, the composite cycled to 7100 and 890, respectively. The creep damage affected the fatigue failure of SiC/SiC composite at elevated temperature.

Ünal et al. (1995) investigated the oxidation on flexural fatigue behavior of 2D CVI Nicalon SiC/SiC composite. After 50 hours oxidation at 1400 °C, the flexural strength at room temperature decreases from 370 to 189 MPa, and the fatigue limit stress decreases from 283 to 130 MPa, due to the formation of SiO_2 strong interface bonding between the fiber and the matrix.

Mizuno et al. (1996) investigated the tensile and fatigue behavior of 2D CVI Nicalon SiC/SiC composite with 0.1 mm PyC interphase at room temperature and 1000 °C in Ar atmosphere. At room temperature, the proportional limit stress is $\sigma_{pls} = 80$ MPa, and the tensile strength is $\sigma_{UTS} = 251$ MPa; and at elevated temperature in Ar atmosphere, the proportional limit stress is $\sigma_{pls} = 100$ MPa, and the tensile strength is $\sigma_{UTS} = 260$ MPa. The tensile strength and failure strain at elevated temperature are higher than those at room temperature, due to the degradation of interface shear stress at elevated temperature in inert atmosphere. However, at elevated temperature in air atmosphere, the tensile strength and fracture strain are both lower than those at room temperature, and the pullout length at the fracture surface is also shorter than that at room temperature, due to the formation of strong interface bonding after interface oxidation. For the cyclic fatigue testing, the loading frequency is $f = 10$ Hz at room temperature, and $f = 20$ Hz at elevated temperature, and the stress ratio is $R = 0.1$, and the maximum cycle number is defined as 10 000 000. At room temperature, the fatigue limit stress is $\sigma_{fls} = 160$ MPa, which is higher than the proportional limit stress (i.e. $\sigma_{pls} = 80$ MPa); and at elevated temperature, the fatigue limit stress is $\sigma_{fls} = 75$ MPa, which is much lower than the proportional limit stress ($\sigma_{pls} = 100$ MPa). The degradation of fatigue limit stress at elevated temperature is attributed to the fiber creep and interface wear.

Zhu et al. (1996, 1997, 1998, 1999) and Zhu and Kagawa (2001) investigated the tensile and fatigue behavior of 2D CVI SiC/SiC composite at room temperature and 1000 °C in Ar atmosphere. At room temperature, the fatigue limit stress is 70–80% tensile strength, which is much higher than the first matrix cracking

stress. Under cyclic fatigue loading, the propagation of matrix cracking is affected by the bridging fibers, and the stress intensity factor decreases due to the bridging effect of the fiber. However, at 1000 °C in Ar atmosphere, the fatigue life decreases greatly, and the fatigue limit stress is $\sigma_{pls} = 75$ MPa, which is about 30% of the tensile strength at elevated temperature.

Zhu (2006) investigated the effect of oxidation of fatigue behavior of 2D CVI SiC/SiC composite. After oxidation for 100 hours at 600 °C, the PyC interphase between the fiber and the matrix disappears, leading to 13% degradation of fatigue life; and after oxidation for 100 hours at 800 °C, the strong interphase of SiO_2 appears between the fiber and the matrix, leading to the shorter fatigue life at room temperature.

Zhu et al. (2004) investigated the low-cyclic fatigue behavior of 3D Tyranno SiC/[Si–Ti–C–O] composite at room temperature. The loading frequencies were $f = 0.02$, 0.2, and 20 Hz, and the fatigue stress ratio was $R = 0.1$ and -0.1. At low loading frequency, the stress corrosion is the main reason for the low-cyclic fatigue failure; and at high loading frequency, the PyC interphase is easy to wear, and the interface debonding length increases with cycles for interface wear, which increases the load carried by the fibers and also decreases the fiber strength, leading to the final fatigue fracture.

Kaneko et al. (2001) and Zhu et al. (2002) investigated the effect of loading frequency on fatigue life of 3D CVI and PIP Tyranno SiC/SiC composites at room temperature. The fibers were coated with nano-scale carbon to decrease interface bonding between fiber and matrix. This coating acts to increase strength and toughness of the composites. The fatigue tests were carried out under load control with a sinusoidal loading frequency of $f = 20$ and 0.2 Hz (PIP SiC/SiC composite) and $f = 20$, 0.2, and 0.02 Hz (CVI SiC/SiC composite) and a stress ratio of $R = 0.1$. There is no difference in fatigue life between 20 and 0.2 Hz for the CVI SiC/SiC composite, but the fatigue life at 0.2 Hz is slightly lower than that at 20 Hz for the PIP SiC/SiC composite, and the fatigue life at 0.02 Hz is much lower than those at 20 and 0.2 Hz for CVI SiC/SiC composite. The fatigue life for PIP SiC/SiC composite is time-dependent at 20–0.2 Hz. For CVI SiC/SiC composite, the fatigue life is time-dependent at 0.2–0.02 Hz, but cyclic-dependent at 20–0.2 Hz. Modulus reduction of PIP SiC/SiC composite saturates after 10 cycles, however, for CVI SiC/SiC composite, the modulus gradual decreases with number of cycles. Because of low sliding stress of PIP SiC/SiC composite, the fatigue strength of PIP SiC/SiC composite is much higher than that of CVI SiC/SiC composite.

Ruggles-Wrenn et al. (2011, 2018) investigated the effect of loading frequency and environment on the fatigue performance of 2D CVI Hi-Nicalon SiC/SiC, CVI Hi-Nicalon SiC/[SiC-B_4C], and MI Hi-Nicalon SiC/SiC composites. The CVI Hi-Nicalon SiC/SiC composite was processed by CVI of SiC into the fiber preforms. Before the infiltration, the fiber preforms were coated with BN fiber coating (~0.25 μm thick) to decrease bonding between the fibers and the matrix. The CVI Hi-Nicalon SiC/[SiC-B_4C] composite had an oxidation inhibited matrix consisting of alternating layers of SiC and B_4C. Prior to infiltration, the fiber preforms were coated with PyC fiber coating (~0.4 μm thick) with boron carbide overlay (~1.0 μm thick) to create a weak fiber/matrix interface. The fiber

preforms of MI Hi-Nicalon SiC/SiC composite were coated with a CVI BN interphase coating, then a CVI SiC coating of initial matrix was applied to rigidize the preforms and to protect the fibers, followed by slurry infiltration of SiC particulates and infiltration of molted Si to fill in the remaining porosity. Under cyclic fatigue loading at 1200 °C in air or in steam condition with the loading frequency of 0.1, 1.0, and 10 Hz, the fatigue life decreases with increasing loading frequency. The material performance degraded rapidly in steam condition. After cyclic fatigue loading in air condition without fatigue failure, the tensile strength at room temperature remained stable, and Young's modulus decreased up to 22%, which indicated that the fiber remained undamaged under cyclic fatigue loading, and the matrix cracking occurred.

The creep property of CMCs is closely related to their constituents and preparation process. For different fiber-reinforced same matrices, the creep property of composite is consistent with the reinforcing fiber. The higher the creep resistance of the fiber, the better the creep resistance of the composite (Morscher 2010). For Tyranno SA, Hi-Nicalon S, and Sylramic-iBN reinforced MI-SiC matrix, the creep resistance of SiC/SiC composite is consistent with that of fiber, i.e. Tyranno SA < Hi-Nicalon S ≤ Sylramic-iBN (Bunsell and Berger 2000; DiCarlo and Yun 2005). For the same fiber-reinforced different densification process matrix, for example, Sylramic-iBN reinforced MI, CVI, PIP SiC matrix, the creep resistance of PIP SiC/SiC composite is the worst, mainly due to the matrix microcracks during fabrication, which decreases the load carrying capacity of the matrix. For the same densification process matrix reinforced by the same fiber, if the matrix components are different, the creep performance of the composite will also be different. For example, for the CVI-G and CVI-H matrix reinforced by Sylramic-iBN fiber, the creep fracture time of the former is only 25 hours at 138 MPa, and the latter is 250 hours, because the matrix of CVI-G is silicon rich, leading to the more prone to creep of the matrix.

Morscher et al. (2008) investigated the retained properties, damage development, and failure mechanisms of 2D MI Sylramic-iBN/BN/SiC composite under tensile creep and fatigue loading. The results show that the retained room temperature tensile strength and modulus decrease with the increase of stress and time. Under different experimental conditions, the failure mechanisms of degradation are different. Under high stress and short time, the oxidation-induced unbridged crack growth emanating from composite surface causes load redistribution in intact region and local stress concentration at matrix crack tip, and eventually one of these cracks develops into fracture pattern with time. Under low stress and long time, the fiber strength degradation is probably due to an intrinsic creep-controlled flaw growth mechanism or attack of the fibers from Si diffusion through the CVI SiC portion of the matrix. However, the matrix cracking stress increases after creep or fatigue test because of the increase of the residual compressive stress of the matrix after the test. For example, for the original composite, the residual compressive stress of the matrix is about 50 MPa, but after tensile creep, the value increases to more than 100 MPa, which is mainly related to the relaxation of the matrix during creep. After unloading, the fiber generates greater compressive stress on the matrix. Therefore, it is necessary to apply more stress to the formation and propagation of matrix cracks to overcome the

existing compressive stress. Although creep or fatigue tests increase the matrix cracking stress, they also increase the number and depth of matrix cracks, which eventually lead to material damage evolution.

In the combustion environment, the fatigue and creep performance and degradation mechanisms are much different from those under air environment. Kim et al. (2010) and Sabelkin (2016) investigated the fatigue and creep performance of 2D MI Hi-Nicalon S SiC/BN/SiC composite under combustion environment and compared with the performance at elevated temperature in air condition. The fatigue life was greater in air condition, approximately by an order of magnitude than in the combustion environment at the same applied peak stress. For example, the fatigue life at the same applied peak stress of 125 MPa was significantly higher in air condition than in the combustion environment, i.e. 58 838 versus 8329 cycles. The creep life decreases about 86% in combustion environment, due to the higher water vapor content in the combustion environment than that in the air condition. The higher water vapor content accelerates the oxidation of BN interphase. At the same time, under the burning of the combustion flame, the compression stress is generated on the front side of the sample, and the tensile stress is generated on the back side. These local thermal stresses reduce the stress threshold of the formation and propagation of the matrix crack, which makes the matrix more prone to crack, providing the channel for the diffusion of oxygen and aggravating the degradation of composite properties.

The degradation behavior of SiC/SiC composites in combustion environment is also affected by the combustion flame temperature and the surface texture of the composite. Bertrand et al. (2015) investigated the tension–tension fatigue behavior of 2D CVI Sylramic-iBN/BN/SiC composite under combustion environment. Fatigue tests were performed at a stress ratio of 0.1 and loading frequency of 1 Hz. The combustion environment was created using a high-velocity oxygen fuel gun, which impinged the flame directly on the one side of specimen when it was subjected to cyclic load. The flame-impinged surface of the specimen was heated top the average temperature of 1250, 1350, and 1480 °C. The SiC/SiC composite achieved a run-out of 25 hours at 46% and 33% of tensile strength under combustion environment at 1250 and 1350 °C, respectively. However, run-out was not achieved at 1480 °C due to erosion and degradation of material. Oxidation embrittlement occurred near the surface on both flame side and backside of the specimen, but more on the flame side. It appears that the make-up of the material, i.e. uneven surface texture, contributed to the increased temperature locally which contributed to the erosion and degradation of the material. The surface texture can be modified with the use of environmental barrier coatings.

1.2.2 Oxide/Oxide CMCs

Oxide/oxide composites possess low density, high-temperature resistance, and oxidation resistance (Zok 2006; Yang et al. 2018). Compared with SiC/SiC composites, oxide/oxide composites have better environmental stability (Lebel et al. 2017; Singh et al. 2017a,2017b), which can serve in the combustion environment

Table 1.4 Properties of oxide fibers.

Fiber	Company	Mass fraction (%)			Diameter (μm)	Strength (MPa)	Modulus (GPa)	Density (g/cm^3)
		Al_2O_3	SiO_2	Other				
Nextel 312	3M	63	25	B_2O_3	10–12	1700	150	2.7
Nextel 440	3M	70	28	B_2O_3	10–12	2000	190	3.1
Nextel 550	3M	73	27	—	10–12	2000	193	3.0
Nextel 610	3M	> 99	<0.3	Fe_2O_3	10–12	3100	380	3.9
Nextel 650	3M	89	—	ZrO_2, Y_2O_3	10–12	2550	358	4.1
Nextel 720	3M	85	15	—	10–12	2100	260	3.4
FP	DuPont	99	—	—	15–25	1400–2100	350–390	3.59
PRD-166	DuPont	80	—	ZrO_2	15–25	2200–2400	85–120	—
Altex	Sumitomo	85	15	—	10/15	1800	210	3.3
Nitivy ALF	Nitivy	72	28	—	7	2000	170	2.9
Saffil	ICI	95	5	—	3	1030	100–300	2.8–3.3

of 1000–1400 °C for a long time (van Roode and Bhattacharya 2013; Askarinejad et al. 2015; Kiser et al. 2015; Lanser and Ruggles-Wrenn 2016; Behrendt et al. 2016).

The preparation methods of oxide/oxide composites include sol–gel method (Sol–Gel), CVI, RMI, PIP process, gel casting (Gelcasting) process, electrophoretic deposition (EPD), etc.

The reinforcing fibers of oxide/oxide composite include Al_2O_3 and Al_2O_3-SiO_2 ceramic fibers. Among commercial oxide fibers, Nextel™ series produced by 3M Company of the United States is the most mature and widely used (Wilson and Visser 2001). In addition, there are FP and PRD-166 series of DuPont company, Altex series of Sumitomo company of Japan, Nitivy ALF series of Nitivy company, and Saffil series of ICI company of the United Kingdom. The basic properties of commonly used oxide fibers are shown in Table 1.4 (Krenkel 2008).

Nextel 312 of 3M Company is the first continuous alumina fiber in the world. Its composition contains Al_2O_3, SiO_2, and B_2O_3. Due to the appearance of glass phase in the fiber, its creep performance is significantly affected, which limits its maximum service temperature. To improve the high-temperature stability of the oxide fiber, 3M Company further reduced the content of B_2O_3 in Nextel 312, and developed Nextel 440, which can be applied to the condition at temperature below 1000 °C, for example, thermal insulation environment. Nextel 550 fiber contains only γ-Al_2O_3 and amorphous SiO_2, and its service temperature is further improved, but it is generally used in the condition at temperature below 1200 °C due to the crystallization temperature of the fiber. To meet the requirements of high-temperature stability of CMCs for hot section components in aerospace, 3M Company has developed Nextel 610 fiber. Nextel 610 is almost completely composed of α-Al_2O_3. At room temperature, it has tensile strength up to 3100 MPa. A small amount of SiO_2 is added to Nextel 610. At high-temperature, it can react

with Al_2O_3 to form mullite and wrap it on the surface of Al_2O_3 grains to prevent the growth of Al_2O_3 grains. Therefore, Nextel 610 still has a strength retention of more than 90% in the high-temperature environment of 1200 °C, but the fiber is easy to creep fracture at temperature above 1300 °C. To improve the creep resistance of the fiber, 3M Company developed Nextel 720™ fiber. Nextel 720 contains 45% α-Al_2O_3 and 55% mullite. Mullite has extremely excellent creep resistance, so the creep resistance of fiber is greatly improved. In addition, 3M Company also developed Nextel 650 fiber, which is mainly composed of α-Al_2O_3. Adding a small amount of ZrO_2 and Y_2O_3 can inhibit the growth of grains and reduce the creep rate. Nextel 650 fiber has better high-temperature tensile strength than Nextel 720, and better creep resistance than Nextel 610.

The matrix materials of oxide/oxide composites mainly include alumina (mainly α-Al_2O_3), mullite ($3Al_2O_3$-$2SiO_2$), yttrium aluminum garnet ($Y_3Al_5O_{12}$ [YAG]), lithium aluminum silicon (LAS), barium aluminum silicon (BAS) glass, etc.

α-Al_2O_3 has moderate sintering temperature, high melting point, excellent mechanical properties, chemical corrosion resistance, and excellent high-temperature oxidation resistance and is widely used as the matrix material of oxide/oxide composites (Ben Ramdane et al. 2017). Ruggles-Wrenn et al. (2006, 2008a,2008b,2008c), Ruggles-Wrenn and Szymczak (2008), Ruggles-Wrenn and Braun (2008), Ruggles-Wrenn and Laffey (2008), Ruggles-Wrenn and Whiting (2011), Lanser and Ruggles-Wrenn (2016), and Ruggles-Wrenn and Lanser (2016) conducted a large number of performance tests on alumina matrix oxide/oxide composites prepared by ATK-COI Ceramic Company, and the results showed that their overall mechanical properties are excellent, but their high-temperature creep resistance is poor. It is easy to cause creep damage of composite materials at elevated temperature.

Mullite ($3Al_2O_3$-$2SiO_2$) is a series of minerals composed of aluminosilicates. It has high melting point, low density, small linear expansion coefficient, stable high-temperature physical and chemical properties, and excellent creep and thermal shock resistance.

The design of oxide/oxide composites mainly uses two basic principles. One is to use an interface layer, generally using a fiber coating; the other is to use a sufficiently weak matrix such as a porous matrix. The fracture behavior of composites is the result of competitive fracture between fibers, interface layers, and the matrix. Tough composites are designed to achieve crack deflection at or near the fiber/matrix interface.

$LaPO_4$ is the most common weak oxide interface layer that meets requirements of crack deflection. $LaPO_4$ has a high melting point (>2000 °C), its bonding with oxides, especially alumina, is weak, and it can coexist stably with oxides such as alumina at high temperatures. Morgan and Marshall (1995) tested the sapphire/$LaPO_4$/alumina composite system and found that the matrix cracks did not penetrate into the fiber, but deflected at the $LaPO_4$/fiber interface. Keller et al. (2003) found that the Nextel 610/Al_2O_3 composite with $LaPO_4$ interface layer has higher strength and service temperature. After heating at 1200 °C for 100 hours, the strength loss of the composite with interface layer is about 28%. After heating at 1200 °C for 1000 hours, the strength retention of the composite still exceeds

60%. However, the strength loss of the composite without interface layer after heating at 1200 °C for five hours is more than 70%. The fracture surface of Nextel 610/$LaPO_4$/Al_2O_3 composite shows that the fiber is pulled out from the alumina matrix, and $LaPO_4$ exists on the pulled fiber surface. However, the composites without interface layer show brittle fracture, and no fiber is pulled out.

The porous interface layer has a pore structure, and the micropores can effectively deflect matrix cracks, thereby consuming the fracture energy of the composite material. Holmquist et al. (2000) carried out research on sapphire/porous ZrO_2/alumina composites. Microcracks existed in the matrix, while the fibers remained intact, which proved that the porous ZrO_2 coating is an effective weak interface layer.

Fugitive coating refers to a type of coating that the interface layer can be removed during the preparation of the composite material. The carbon interface layer in the oxide/oxide composite can be removed by oxidation before or during use, leaving gaps at the fiber/matrix interface. Keller et al. (2000) showed that fugitive carbon interface layers can provide weak interface layers for sapphire/YAG and Nextel 720/calcium aluminosilicate (CAS) composites.

In the design of oxide/oxide composites, a relatively weak matrix is currently widely used to replace the fiber/matrix interface layer. In porous matrix composites, cracks in the matrix are deflected in the matrix at the fiber/matrix interface. Compared with a dense matrix, the porous matrix does not cause stress concentration on the fiber surface to break the fiber. Although the bond between the fibers and the matrix particles is strong, cracks generally develop toward adjacent pores and eventually reach the fiber surface in the pores, resulting in deflection.

Steel et al. (2001) investigated the tensile and tension–tension fatigue behavior of PIP 8HSW Nextel 720/alumina composite at room temperature and 1200 °C in air atmosphere. The fatigue tests were under load control with the loading frequency of $f = 1$ Hz, stress ratio of $R = 0.05$, and the maximum applied cycle number of $N = 100\,000$. At room temperature, the tensile strength is $\sigma_{UTS} = 144$ MPa, and the fatigue limit stress is $\sigma_{pls} = 102$ MPa, which is 70% of tensile strength. At 1200 °C in air condition, the tensile strength is $\sigma_{UTS} = 140$ MPa, and the fatigue limit stress is $\sigma_{pls} = 122$ MPa, which is 87% of tensile strength. The fatigue damage mechanisms at elevated temperature are similar with those at room temperature; however, the fiber creep also affects the fatigue damage.

Zawada et al. (2003) investigated the tensile, shear, fatigue and creep behavior of 2D Nextel 610/Al_2O_3-SiO_2 composite at room temperature and 1000 °C in air atmosphere. The fatigue loading frequency is $f = 1$ Hz, stress ratio is $R = 0.05$, and maximum applied cycle is $N = 100\,000$. At room temperature, the fatigue limit stress is $\sigma_{pls} = 170$ MPa, which is 85% of tensile strength; at 1000 °C in air atmosphere, the fatigue limit stress is $\sigma_{pls} = 150$ MPa, which is 85% of tensile strength. At elevated temperature, when the fatigue peak stress is between $\sigma_{max} = 100$ and 150 MPa, the modulus decreases 5–10% during first 1000 cycles, and then the modulus remains constant till the maximum applied cycle number, which indicates that there is no obvious damage accumulation under cyclic fatigue loading. The energy dissipation for each cycle is very low, only 3–5 kJ/m^3. When the fatigue peak stress is $\sigma_{max} = 150$ MPa, the strain range remains unchanged with

increasing cycles, which indicates that there is little damage accumulation during cyclic fatigue loading. After experiencing 100 000 cycles under $\sigma_{max} = 150$ MPa at elevated temperature, the tensile strength at room temperature is the same with that of original specimen; however, the modulus decreases mainly due to matrix cracking. The oxide/oxide composite has good fatigue and oxidation resistance at high temperatures.

Mall and Ahn (2008) investigated the effect of loading frequency on tension–tension fatigue behavior of 2D Nextel 720/alumina composite at room temperature. The fatigue tests were controlled under load with the stress ratio of $R = 0.05$, and the loading frequency of $f = 1$, 100, and 900 Hz, and the corresponding maximum cycle number is $N = 100\,000$, 100 000 000, and 100 000 000. When the loading frequency increases from $f = 1$–900 Hz, the fatigue life increases with loading frequency. When the fatigue peak stress is $\sigma_{max} = 120$ MPa, the fatigue cycle number is $N = 600$, 6000, and 100 000 000 for the loading frequency of $f = 1$, 100, and 900 Hz. Fatigue behavior of Nextel 720/alumina appeared to be a combination of cycle-dependent and time-dependent phenomena. Surface temperature of specimens tested at 900 Hz increased considerably relative to that at 1 or 100 Hz (70 °C versus 5 °C increase). Damage mechanisms showed an evidence of local fiber/matrix interfacial bonding developed during cycling due to frictional heating at the highest frequency of 900 Hz. This was not observed at the two lower frequencies. This interfacial bonding may have caused an increase in fatigue life/strength of the tested CMC system at the highest frequency of 900 Hz.

Ruggles-Wrenn et al. (2008a) investigated the effect of loading frequency on fatigue life of 2D Nextel 720/alumina composite at 1200 °C in air and in steam environment. In air condition, the loading frequency is $f = 0.1$ and 1 Hz, and the fatigue peak stress is between $\sigma_{max} = 100$ and 170 MPa, and the maximum applied cycle number is $N = 100\,000$; in steam atmosphere, the loading frequency is $f = 0.1$, 1, and 10 Hz, and the fatigue peak stress is between $\sigma_{max} = 75$ and 170 MPa, and the maximum applied cycle number for the loading frequency of $f = 0.1$ and 1 Hz is $N = 100\,000$, and the maximum applied cycle number of the loading frequency of $f = 10$ Hz is $N = 1\,000\,000$. In air condition, the loading frequency of $f = 0.1$ and 1.0 Hz has little effect on the fatigue life, and the fatigue limit stress is $\sigma_{pls} = 170$ MPa, which is 88% of the tensile strength. After fatigue loading, the residual strength remains unchanged, however, the modulus decreases about 30%. In steam condition, the loading frequency affects the fatigue life. When the loading frequency is $f = 10$ Hz, the fatigue limit stress is $\sigma_{pls} = 150$ MPa, which is 78% of the tensile strength. After fatigue loading, the residual strength decreases about 4%, and the modulus decreases about 7%. When the loading frequency is $f = 1$ Hz, the fatigue limit stress is $\sigma_{pls} = 125$ MPa, which is 69% of the tensile strength. After fatigue loading, the residual strength decreases about 12%, and the modulus decreases about 20%. However, for the loading frequency of $f = 0.1$ Hz, the fatigue limit stress is lower than 75 MPa. On the fracture surface, there exists a lot of fiber pullout for the loading frequency of $f = 10$ Hz, and few fiber pullout for the loading frequency of $f = 0.1$ Hz.

1.3 The Function of Interface in Ceramic-Matrix Composites

In CMCs, the interphase is usually used to control the bonding strength between the fiber and the matrix. The mechanical behavior of CMCs depends not only on the properties of the fiber and the matrix, but also on the interface bonding strength between the fiber and the matrix. If the bonding strength between the fiber and the matrix is too high, the stress concentration will make the fiber unable to carry load uniformly, resulting in low strength of CMCs. At the same time, due to the lack of energy absorption mechanism in the process of fracture, the toughness of CMC is low. Therefore, only when the bonding strength between the fiber and the matrix is moderate, the fiber can not only effectively bear the load, but also consume energy through debonding and pulling out in the process of fracture, so as to realize the strengthening and toughening of CMC. Because of the existence of the interface layer, the CMCs can have ductile fracture. The toughening mechanisms of CMCs include crack deflection, fiber debonding, fiber bridging, and fiber pullout. Fiber pullout is the main toughening mechanism of composite materials. Through the friction energy consumption in the process of fiber pullout, the fracture work of composite materials increases, while the energy consumption in the process of fiber pullout depends on the fiber pullout length and the sliding resistance of debonding surface. The sliding resistance is too large, the fiber pullout length is short, the toughening effect is not good, and the strength is low. The pullout length of the fiber depends on the strength distribution of the fiber and the sliding resistance of the interface, while the sliding resistance mainly depends on the interface layer and the surface roughness of the fiber.

Under tensile loading of CMCs, matrix cracking and interface debonding occur, and the fiber and matrix stress distribution can be determined using the shear-lag theory.

When the stress in the matrix approaches the matrix strength, matrix will crack. When the interface completely debonds, the stress in the matrix cannot approach the matrix strength, and the matrix cracking approaches saturation. During matrix cracking evolution, the process includes the first matrix cracking and the saturation of matrix cracking.

For the CMC system, the core of its strengthening and toughening is the optimal design of interphase. The interface phase has two basic functions. One is mechanical fuse function that is to deflect crack growth to protect the fiber, which is the most basic function of the interphase. The second is the load transfer function, which transfers the load to the fiber through shear. In addition to the aforementioned two basic functions, the interphase also plays a buffer role, which is to absorb the residual thermal stress generated due to the mismatch of the thermal expansion coefficient of the fiber and the matrix. In order to achieve this function, the interphase must be thick enough to have a compliant. Because most CMCs are used in high-temperature oxidizing atmosphere, the microcracks

in the matrix will accelerate the diffusion of oxidizing atmosphere to the internal interphase and fibers, which requires the interphase to have oxidation resistance.

1.3.1 Effect of Interphase on Sliding Resistance

The introduction of interphase can change the roughness of debonding surface, the interphase can change the interaction surface between fiber and matrix, and the increase of interphase thickness can weaken the engagement strength in the process of sliding, and reduce the frictional resistance of sliding. If the interphase thickness exceeds the roughness amplitude, the friction stress can be almost eliminated. In addition, the crystallization of the interphase after high-temperature treatment will increase, for example, the graphitization of the PyC interphase after heat treatment will increase, which will also help the interface slip and reduce the slip resistance.

1.3.2 Effect of Interphase on Thermal Misfit Stress

Interphase can adjust the thermal residual stress (TRS) between the fiber and the matrix. The thermal expansion coefficient and thickness of interphase affect the TRS (Kuntz et al. 1993).

Ignore the influence of the geometry and the elastic constants of the fiber; the fiber radial TRS can be determined using the following equation.

$$\sigma_{\mathrm{r}} = E_{\mathrm{m}} \Delta T \Delta \alpha \tag{1.5}$$

The factors in Eq. (1.5) are defined as follows: $\Delta T = T - T_0$, where T_0 is the stress-free temperature (e.g. the fabrication temperature) and T is the temperature at which the stress is determined. Usually, $\Delta T < 0$, when T_0 is the fabrication temperature. $\Delta \alpha = \alpha_{\mathrm{m}} - \alpha_{\mathrm{f}}$, where α is the thermal expansion coefficient and the subscripts f and m refer to the fiber and the matrix, respectively. The radial stresses become negative (pressure) when $\alpha_{\mathrm{m}} > \alpha_{\mathrm{f}}$ or positive (tension), when $\alpha_{\mathrm{m}} < \alpha_{\mathrm{f}}$. E_{m} is Young's modulus of the matrix. Faber (1997), Kuntz et al. (1993), Davis et al. (1993), Brennan (1990), and Kerans (1996) developed methods to calculate the TRS; however, these calculations were conducted without considering the thickness of the interphase.

For the SiC/PyC/borosilicate glass composite, the modulus of interphase is about 80 GPa, and the thickness is about 80 nm. The thermal expansion coefficient of PyC interphase has a significant effect on the axial and circumferential residual stresses in PyC, and the effect on the radial residual stresses can be ignored. The thermal expansion coefficient of interphase has a significant effect on the TRS in fiber and interphase, but the effect on matrix TRS is small (Kuntz et al. 1993).

1.4 The Design of Interface in Ceramic-Matrix Composites

Interphase plays an important role in CMCs, but not all high-temperature materials can be used as interphase materials, which need to meet three conditions:

(1) Low modulus. The low modulus can reduce the mismatch of thermal expansion coefficient and modulus between the fiber and the matrix, thus reducing the physical damage of fiber.
(2) Low shear strength. Because the interface is the place where the matrix cracks deflect, the interphase should have low shear strength, which can realize the crack deflection, fiber pullout, debonding, and other toughening mechanisms.
(3) High thermal and chemical stability. It can prevent the fiber from being damaged in the process of composite preparation, and it can exist stably in the process of composite service.

There are few interphase materials that can meet the above conditions. This kind of materials is usually composed of layered crystal materials. The bonding force between layers is weak, and the direction of the lamellae is parallel to the fiber surface. Commonly used are PyC interphase and BN interphase.

1.4.1 PyC Interphase

PyC is a traditional and common interphase of CMCs, and it is the first interphase that can produce toughness in ceramic fiber-reinforced CMCs. The in situ growth of carbon interphase on the fiber surface can make the weak interface between the fiber and the matrix, thus improving the fracture toughness of the composite. The toughness of the composite increases with the increase of the thickness of the interphase, but the load transfer between the matrix and the fiber decreases with the increase of interphase thickness. Therefore, the interphase thickness is generally 0.1–0.3 μm.

The use of a PyC interphase can significantly improve the performance of composite materials at room temperature or in a high-temperature inert atmosphere, but PyC begins to oxidize at 400 °C in air atmosphere, and CMC materials are mostly used in air atmosphere. The PyC interphase is not an ideal interphase. Generally, the PyC interphase requires the matrix to have a high dense level, so that the fiber does not directly contact the outside oxidizing atmosphere, or one or more dense protective layers are deposited on the PyC surface. In the case of cracking occurrence, the PyC interphase is still easy to damage.

Filipuzzi and Naslain (1994) and Filipuzzi et al. (1994) studied the interphase oxidation in Nicalon SiC/PyC/SiC composites. Carbon is oxidized to generate CO and CO_2 gas. After the gas is released, a gap is left between the fiber and the matrix, causing adjacent fibers and the matrix to oxidize and generate SiO_2. Oxygen diffuses along the voids that occur during the oxidation of the fibers and the matrix, resulting in continuous oxidation of the composite material until the SiO_2 generated by the oxidation of the fibers and the matrix closes the voids. According to the oxidation rate constants of Nicalon fibers and SiC matrix, Luthra (1994)

calculated the time required to close the voids and found that it increase with the increase in the thickness of the interphase.

Non-oxide CMCs are designed to operate below the proportional limit stress, but it should be considered that they sometimes operate at temperatures above the proportional limit stress. When this happens, oxygen diffuses along the matrix cracks and oxidizes the PyC interphase.

1.4.2 BN Interphase

In addition to PyC, BN is the only fiber coating capable of slow failure in non-oxide composites. It should be noted that not all BNs are the same. When deposited at low temperature, the generated BN is amorphous; when deposited at high temperature (for example, above 1500 °C), BN generally has an ordered hexagonal crystal structure (which can make CMCs exhibit tough behavior). The deposited BN must contain carbon or oxygen; and the silicon-doped BN has higher oxidation resistance.

As CMCs with PyC interphase, the toughness of CMCs with BN interphase increases with coating thickness. The optimal thickness range of BN interphase should be 0.3–0.5 μm, which is thicker than PyC interphase.

Since the oxidation products of BN are liquid boron oxide rather than gaseous oxide, it is expected that the oxidation rate of BN in dry air or oxygen is much lower than that of carbon. The oxidation depth of the BN coating of the SiC-Si matrix composite material observed in the experiment is very shallow. When the oxidation is performed at a temperature range of 700–1200 °C for 100 hours, the oxidation depth is only in the order of 10 μm or less. The oxidation depth of BN coating is much shallower than that of PyC coating. In dry oxidizing environments, BN coatings perform better than PyC coatings.

Oxidation experiments in a humid environment show that the oxidation properties of BN coatings are similar to those of carbon coatings. When the matrix is cracked, oxidants (oxygen and water vapor) can quickly diffuse through the matrix cracks and oxidize the fiber coating. Generally the thickness of the coating does not exceed 1 μm. As a result, the coating will oxidize rapidly, only a few minutes at an experimental temperature above 900 °C (Jacobson et al. 1999), and this damage will quickly spread to the fibers.

1.5 Conclusion

In this chapter, the definition, function, and design of interface in different fiber-reinforced CMCs are given. The interphase plays an important role in the mechanical behavior of non-oxide and oxide/oxide CMCs at room and elevated temperatures. The interface phase has two basic functions: one is mechanical fuse function that is to deflect crack growth to protect the fiber, which is the most basic function of the interphase. The second is the load transfer function, which transfers the load to the fiber through shear. In addition to the aforementioned two basic functions, the interphase also plays a buffer role, which is to absorb the

residual thermal stress generated due to the mismatch of the thermal expansion coefficient of the fiber and the matrix. The characteristics of PyC interphase and BN interphase used in CMCs are also analyzed.

References

Askarinejad, S., Rahbar, N., Sabelkin, V., and Mall, S. (2015). Mechanical behavior of a notched oxide/oxide ceramic matrix composite in combustion environment: experiments and simulations. *Composite Structures* 127: 77–86. https://doi.org/10.1016/j.compstruct.2015.02.040.

Behrendt, T., Hackemann, S., Mechnich, P. et al. (2016). Development and test of oxide/oxide ceramic matrix composites combustor liner demonstrators for aero-engines. *Journal of Engineering for Gas Turbines and Power* 139: 031705. https://doi.org/10.1115/1.4034515.

Ben Ramdane, C., Julian-Jankowiak, A., Valle, R. et al. (2017). Microstructure and mechanical behaviour of a Nextel™ 610/alumina weak matrix composite subjected to tensile and compressive loadings. *Journal of the European Ceramic Society* 37: 2919–2932. https://doi.org/10.1016/j.jeurceramsoc.2017.02.042.

Bertrand, D.J., Sabelkin, V., Zawada, L., and Mall, S. (2015). Fatigue behavior of sylramic-iBN/BN/CVI SiC ceramic matrix composite in combustion environment. *Journal of Materials Science* 50: 7437–7447. https://doi.org/10.1007/s10853-015-9302-8.

Brennan, J.J. (1990). Interfacial studies of chemical-vapor-infiltrated ceramic matrix composites. *Materials Science and Engineering A* 126: 203–223. https://doi.org/10.1016/0921-5093(90)90126-N.

Bunsell, A.R. and Berger, M.H. (2000). Fine diameter ceramic fibers. *Journal of the European Ceramic Society* 20: 2249–2260. https://doi.org/10.1016/S0955-2219(00)00090-X.

Chawla, N., Holmes, J.W., and Lowden, R.A. (1996). The role of interfacial coatings on the high frequency fatigue behavior of Nicalon/C/SiC composites. *Scripta Materialia* 35: 1411–1416. https://doi.org/10.1016/S1359-6462(96)00326-0.

Corman, G., Upadhyay, R., Sinha, S. et al. (2016). General electric company: selected applications of ceramics and composite materials. In: *Materials Research for Manufacturing: An Industrial Perspective of Turning Materials into New Products*. Cham, Switzerland: Springer International Publishing. https://doi.org/10.1007/978-3-319-23419-9_3.

Davis, J.B., Löfvander, J., Evans, A.G. et al. (1993). Fiber coating concepts for brittle-matrix composites. *Journal of the American Ceramic Society* 76: 1249–1257. https://doi.org/10.1111/j.1151-2916.1993.tb03749.x.

DiCarlo, J.A. and Yun, H.M. (2005). Non-oxide (silicon carbide) fibers. In: *Handbook of Ceramic Composites* (ed. N.P. Bansal). Boston, MA: Springer. https://doi.org/10.1007/0-387-23986-3_2.

Elahi, M., Liao, K., Lesko, J. et al. (1996). Elevated temperature cyclic fatigue of silicon carbide fiber reinforced silicon carbide matrix composites. In: *Ceramic Engineering and Science Proceedings*, vol. 17, 357–361. https://doi.org/10.1002/9780470314500.ch1.

Faber, K.T. (1997). Ceramic composite interfaces: properties and design. *Annual Review of Materials Science* 27: 499–524. https://doi.org/10.1146/annurev.matsci.27.1.499.

Filipuzzi, L. and Naslain, R. (1994). Oxidation mechanisms and kinetics of 1D-SiC/C/SiC composite materials: II. Modeling. *Journal of the American Ceramic Society* 77: 467–480. https://doi.org/10.1111/j.1151-2916.1994.tb07016.x.

Filipuzzi, L., Camus, G., Naslain, R., and Thebault, J. (1994). Oxidation mechanisms and kinetics of 1D-SiC/C/SiC composite materials: I. An experimental approach. *Journal of the American Ceramic Society* 77: 459–466. https://doi.org/10.1111/j.1151-2916.1994.tb07015.x.

Holmquist, M., Lundberg, R., Sudre, O. et al. (2000). Alumina/alumina composite with a porous zirconia interphase – processing, properties and component testing. *Journal of the European Ceramic Society* 20: 599–606. https://doi.org/10.1016/S0955-2219(99)00258-7.

Jacobson, N., Farmer, S., Moore, A., and Sayir, H. (1999). High-temperature oxidation of boron nitride: I. Monolithic boron nitride. *Journal of the American Ceramic Society* 82: 393–398. https://doi.org/10.1111/j.1551-2916.1999.tb20075.x.

Kaneko, Y., Zhu, S., Ochi, Y. et al. (2001). Effect of frequency on fatigue behavior in Tyranno fiber reinforced SiC composites. In: *Ceramic Engineering and Science Proceedings*, vol. 22, 553–560. https://doi.org/10.1002/9780470294680.ch64.

Keller, K.A., Mah, T.I., Parthasarathy, T.A., and Cooke, C.M. (2000). Fugitive interfacial carbon coatings for oxide/oxide composites. *Journal of the American Ceramic Society* 83: 329–336. https://doi.org/10.1111/j.1151-2916.2000.tb01194.x.

Keller, K.A., Mah, T.I., Parthasarathy, T.A. et al. (2003). Effectiveness of monazite coatings in oxide/oxide composites after long-term exposure at high temperature. *Journal of the American Ceramic Society* 86: 325–332. https://doi.org/10.1111/j.1151-2916.2003.tb00018.x.

Kerans, R.J. (1996). Viability of oxide fiber coatings in ceramic composites for accommodation of misfit stresses. *Journal of the American Ceramic Society* 79: 1664–1668. https://doi.org/10.1111/j.1151-2916.1996.tb08779.x.

Kim, T.T., Mall, S., Zawada, L.P., and Jefferson, G. (2010). Simultaneous fatigue and combustion exposure of a SiC/SiC ceramic matrix composite. *Journal of Composite Materials* 44: 2991–3016. https://doi.org/10.1177/0021998310373519.

Kiser, J.D., Bansal, N.P., Szelagowski, J., et al. (2015). Oxide/oxide ceramic matrix composite (CMC) exhaust mixer development in the NASA environmentally responsible aviation (ERA) project. *Proceedings of ASME Turbo Expo 2015: Turbine Technical Conference and Exposition*, Montreal, Quebec, Canada (15–19 June 2015). New York: ASME.

Krenkel, W. (ed.) (2008). *Ceramic Matrix Composites: Fiber-Reinforced Ceramics and Their Applications*. Weinheim: Wiley-VCH. https://doi.org/10.1002/9783527622412.

Kuntz, M., Meier, B., and Grathwohl, G. (1993). Residual stresses in fiber-reinforced ceramics due to thermal expansion mismatch. *Journal of the American Ceramic Society* 76: 2607–2612. https://doi.org/10.1111/j.1151-2916.1993.tb03988.x.

Lanser, R.L. and Ruggles-Wrenn, M.B. (2016). Tension-compression fatigue of a Nextel™ 720/alumina composite at 1200 °C in air and in steam. *Applied Composite Materials* 23: 707–717. https://doi.org/10.1007/s10443-016-9481-8.

Lebel, L., Turenne, S., and Boukhili, R. (2017). An experimental apparatus and procedure for the simulation of thermal stresses in gas turbine combustion chamber panels made of ceramic matrix composites. *Journal of Engineering for Gas Turbines and Power* 139: 091502. https://doi.org/10.1115/1.4035906.

Li, L. (2018). *Damage, Fracture and Fatigue of Ceramic-Matrix Composites*. Springer Nature Singapore Private Limited. ISBN: 978-981-13-1782-8. https://doi.org/10.1007/978-981-13-1783-5.

Li, L. (2019). *Thermomechanical Fatigue of Ceramic-Matrix Composites*. Wiley-VCH. ISBN: 978-3-527-34637-0. https://onlinelibrary.wiley.com/doi/book/10.1002/9783527822614.

Liu, H., Yang, J., Zhou, Y. et al. (2018). Progress in coupon tests of SiC_f/SiC ceramic matrix composites used for aero engines. *Journal of Materials Engineering* 46: 1–12.

Luthra, K.L. (1994). Theoretical aspects of the oxidation of silica-forming ceramics. In: *Corrosion of Advanced Ceramics*, NATO Science Series E: (Closed), vol. 267 (ed. K.G. Nickel). Dordrecht: Springer. https://doi.org/10.1007/978-94-011-1182-9_2.

Mall, S. and Ahn, J.M. (2008). Frequency effects on fatigue behavior of Nextel 720™ /alumina at room temperature. *Journal of the European Ceramic Society* 28: 2783–2789. https://doi.org/10.1016/j.jeurceramsoc.2008.04.005.

Mizuno, M., Zhu, S., Nagano, Y. et al. (1996). Cyclic-fatigue behavior of SiC/SiC composites at room and high temperatures. *Journal of the American Ceramic Society* 79: 3065–3077. https://doi.org/10.1111/j.1151-2916.1996.tb08078.x.

Morgan, P.E.D. and Marshall, D.B. (1995). Ceramic composites of monazite and alumina. *Journal of the American Ceramic Society* 78: 1553–1563. https://doi.org/10.1111/j.1151-2916.1995.tb08851.x.

Morscher, G.N. (2010). Tensile creep and rupture of 2D-woven SiC/SiC composites for high temperature applications. *Journal of the European Ceramic Society* 30: 2209–2221. https://doi.org/10.1016/j.jeurceramsoc.2010.01.030.

Morscher, G.N., Hurst, J., and Brewer, D. (2000). Intermediate-temperature stress rupture of a woven Hi-Nicalon, BN-interphase, SiC-matrix composite in air. *Journal of the American Ceramic Society* 83: 1441–1449. https://doi.org/10.1111/j.1151-2916.2000.tb01408.x.

Morscher, G.N., Ojard, G., Miller, R. et al. (2008). Tensile creep and fatigue of Sylramic-iBN melt-infiltrated SiC matrix composites: retained properties, damage development, and failure mechanisms. *Composites Science and Technology* 68: 3305–3313. https://doi.org/10.1016/j.compscitech.2008.08.028.

Nasiri, N.A., Patra, N., Ni, N. et al. (2016). Oxidation behaviour of SiC/SiC ceramic matrix composites in air. *Journal of the European Ceramic Society* 36: 3293–3302. https://doi.org/10.1016/j.jeurceramsoc.2016.05.051.

Reynaud, P. (1996). Cyclic fatigue of ceramic-matrix composites at ambient and elevated temperatures. *Composites Science and Technology* 56: 809–814. https://doi.org/10.1016/0266-3538(96)00025-5.

Reynaud, P., Rouby, D., and Fantozzi, G. (1994). Effects of interfacial evolutions on the mechanical behaviour of ceramic matrix composites during cyclic fatigue. *Scripta Metallurgica et Materialia* 31: 1061–1066. https://doi.org/10.1016/0956-716X(94)90527-4.

van Roode, M. and Bhattacharya, A.K. (2013). Durability of oxide/oxide ceramic matrix composites in gas turbine combustors. *Journal of Engineering for Gas Turbines and Power* 135: 051301. https://doi.org/10.1115/1.4007978.

Rouby, D. and Reynaud, P. (1993). Fatigue behaviour related to interface modification during load cycling in ceramic-matrix fibre composites. *Composites Science and Technology* 48: 109–118. https://doi.org/10.1016/0266-3538(93)90126-2.

Roy, J., Chandra, S., Das, S., and Maitra, S. (2014). Oxidation behaviour of silicon carbide – a review. *Reviews on Advanced Materials Science* 38: 29–39.

Ruggles-Wrenn, M.B. and Braun, J.C. (2008). Effects of steam environment on creep behavior of Nextel™ 720/alumina ceramic composite at elevated temperature. *Materials Science and Engineering A* 497: 101–110. https://doi.org/10.1016/j.msea.2008.06.036.

Ruggles-Wrenn, M.B. and Laffey, P. (2008). Creep behavior in interlaminar shear of Nextel™ 720/alumina ceramic composite at elevated temperature in air and in steam. *Composites Science and Technology* 68: 2260–2266. https://doi.org/10.1016/j.compscitech.2008.04.009.

Ruggles-Wrenn, M.B. and Lanser, R.L. (2016). Tension-compression fatigue of an oxide/oxide ceramic composite at elevated temperature. *Materials Science and Engineering A* 659: 270–277. https://doi.org/10.1016/j.msea.2016.02.057.

Ruggles-Wrenn, M.B. and Szymczak, N.R. (2008). Effects of steam environment on compressive creep behavior of Nextel™ 720/alumina ceramic composite at 1200 °C. *Composites Part A Applied Science and Manufacturing* 39: 1829–1837. https://doi.org/10.1016/j.compositesa.2008.09.005.

Ruggles-Wrenn, M.B. and Whiting, B.A. (2011). Cyclic creep and recovery behavior of Nextel™ 720/alumina ceramic composite at 1200 °C. *Materials Science and Engineering A* 528: 1848–1856. https://doi.org/10.1016/j.msea.2010.10.011.

Ruggles-Wrenn, M.B., Mall, S., Eber, C.A., and Harlan, L.B. (2006). Effects of steam environment on high-temperature mechanical behavior of Nextel™ 720/alumina (N720/A) continuous fiber ceramic composite. *Composites Part A Applied Science and Manufacturing* 37: 2029–2040. https://doi.org/10.1016/j.compositesa.2005.12.008.

Ruggles-Wrenn, M.B., Hetrick, G., and Baek, S.S. (2008a). Effects of frequency and environment on fatigue behavior of an oxide–oxide ceramic composite at 1200 °C. *International Journal of Fatigue* 30: 502–516. https://doi.org/10.1016/j.ijfatigue.2007.04.004.

Ruggles-Wrenn, M.B., Radzicki, A.T., Baek, S.S., and Keller, K.A. (2008b). Effect of loading rate on the monotonic tensile behavior and tensile strength of an oxide–oxide ceramic composite at 1200 °C. *Materials Science and Engineering A* 492: 88–94. https://doi.org/10.1016/j.msea.2008.03.006.

Ruggles-Wrenn, M.B., Siegert, G.T., and Baek, S.S. (2008c). Creep behavior of Nextel™ 720/alumina ceramic composite with ±45° fiber orientation at 1200 °C.

Composites Science and Technology 68: 1588–1595. https://doi.org/10.1016/j.compscitech.2007.07.012.

Ruggles-Wrenn, M.B., Christensen, D.T., Chamberlain, A.L. et al. (2011). Effect of frequency and environment on fatigue behavior of a CVI SiC/SiC ceramic matrix composite at 1200 °C. *Composites Science and Technology* 71: 190–196. https://doi.org/10.1016/j.compscitech.2010.11.008.

Ruggles-Wrenn, M.B., Boucher, N., and Przybyla, C. (2018). Fatigue of three advanced SiC/SiC ceramic matrix composites at 1200 °C in air and in steam. *International Journal of Applied Ceramic Technology* 15: 3–15.

Sabelkin, V., Mall, S., Cook, T.S., and Fish, J. (2016). Fatigue and creep behaviors of a SiC/SiC composite under combustion and laboratory environments. *Journal of Composite Materials* 50: 2145–2153. https://doi.org/10.1177/0021998315602323.

Singh, A.K., Sabelkin, V., and Mall, S. (2017a). Fatigue behavior of double-edge notched oxide/oxide ceramic matrix composite in a combustion environment. *Journal of Composite Materials* 51: 3669–3683. https://doi.org/10.1177/0021998317692655.

Singh, A.K., Sabelkin, V., and Mall, S. (2017b). Creep-rupture behaviour of notched oxide/oxide ceramic matrix composite in combustion environment. *Advances in Applied Ceramics* 117: 30–41. https://doi.org/10.1080/17436753.2017.1359444.

Steel, S.G., Zawada, L.P., and Mall, S. (2001). Fatigue behavior of a Nextel™ 720/alumina (N720/A) composite at room and elevated temperature. In: *Ceramic Engineering and Science Proceedings*, vol. 22, 695–702. https://doi.org/10.1002/9780470294680.ch80.

Ünal, Ö. (1996a). Cyclic tensile stress-strain behaviour of SiC/SiC composites. *Journal of Materials Science Letters* 15: 789–791. https://doi.org/10.1007/BF00274605.

Ünal, Ö. (1996b). Tensile and fatigue behavior of a SiC/SiC composite at 1300 °C. In: *Symposium on Thermal and Mechanical Test Methods and Behavior of Continuous-Fiber Ceramic Composites* (ASTM-STP-1309). Philadelphia: American Society for Testing and Materials. https://doi.org/10.2172/238543.

Ünal, Ö. (1996c). Low-cycle tensile fatigue behavior of a SiC/SiC composite. In: *Ceramic Engineering and Science Proceedings*, vol. 17, 157–165. https://doi.org/10.1002/9780470314876.ch16.

Ünal, Ö., Eckel, A.J., and Laabs, F.C. (1995). The 1400 °C-oxidation effect on microstructure, strength and cyclic life of SiC/SiC composites. *Scripta Metallurgica et Materialia* 33: 983–988. https://doi.org/10.1016/0956-716X(95)00309-J.

Wilson, D.M. and Visser, L.R. (2001). High performance oxide fibers for metal and ceramic composites. *Composites Part A Applied Science and Manufacturing* 32: 1143–1153. https://doi.org/10.1016/S1359-835X(00)00176-7.

Yang, R., Qi, Z., Yang, J., and Jiao, J. (2018). Research progress in oxide/oxide ceramic matrix composites and processing technologies. *Journal of Materials Engineering* 46: 1–9.

Zawada, L.P., Hay, R.S., Lee, S.S., and Staehler, J. (2003). Characterization and high-temperature mechanical behavior of an oxide/oxide composite. *Journal of the American Ceramic Society* 86: 981–990. https://doi.org/10.1111/j.1151-2916.2003.tb03406.x.

Zhu, S. (2006). Fatigue behavior of ceramic matrix composite oxidized at intermediate temperatures. *Materials Transactions* 47: 1965–1967. https://doi.org/10.2320/matertrans.47.1965.

Zhu, S. and Kagawa, Y. (2001). Fatigue fracture in SiC fiber reinforced SiC composites. *Seisan Kenkyu* 53: 40–43. https://doi.org/10.11188/seisankenkyu.53.470.

Zhu, S., Kagawa, Y., Mizuno, M. et al. (1996). In situ observation of cyclic fatigue crack propagation of SiC-fiber/SiC composite at room temperature. *Materials Science and Engineering A* 220: 100–107. https://doi.org/10.1016/S0921-5093(96)10440-8.

Zhu, S., Mizuno, M., Kagawa, Y. et al. (1997). Creep and fatigue behavior of SiC fiber reinforced SiC composite at high temperatures. *Materials Science and Engineering A* 225: 69–77. https://doi.org/10.1016/S0921-5093(96)10872-8.

Zhu, S., Mizuno, M., Nagano, Y. et al. (1998). Creep and fatigue behavior of enhanced SiC/SiC composite at high temperatures. *Journal of the American Ceramic Society* 81: 2269–2277. https://doi.org/10.1111/j.1151-2916.1998.tb02621.x.

Zhu, S., Mizuno, M., Kagawa, Y., and Mutoh, Y. (1999). Monotonic tension, fatigue and creep behavior of SiC-fiber-reinforced SiC-matrix composites: a review. *Composites Science and Technology* 59: 833–851. https://doi.org/10.1016/S0266-3538(99)00014-7.

Zhu, S., Kaneko, Y., Ochi, Y. et al. (2002). Effect of frequency on fatigue behavior in 3D-woven Tyranno fiber reinforced SiC composites. *Journal of the Society of Materials Science Japan* 51: 1400–1404. https://doi.org/10.2472/jsms.51.1400.

Zhu, S., Kaneko, Y., Ochi, Y. et al. (2004). Low cycle fatigue behavior in an orthogonal three-dimensional woven Tyranno fiber reinforced Si–Ti–C–O matrix composite. *International Journal of Fatigue* 26: 1069–1074. https://doi.org/10.1016/j.ijfatigue.2004.03.001.

Zok, F.W. (2006). Developments in oxide fiber composites. *Journal of the American Ceramic Society* 89: 3309–3324. https://doi.org/10.1111/j.1551-2916.2006.01342.x.